A Preliminary Study of Quantitative Protocols in Indium 111 SPECT Using Computational Simulations and Phantoms

Karine Assié, Arnaud Dieudonné, Isabelle Gardin, Pierre Véra, and Irene Buvat

Abstract—Indium 111 SPECT allows one to determine the activity distribution of tracers used in radioimmunotherapy, such as Zevalin® labeled with yttrium 90. Using computer simulations and phantom models, we assessed various processing schemes to identify a clinically feasible protocol to estimate the tracer concentrations from ^{111}In SPECT images.

The SPECT acquisition of a cylindrical phantom containing spheres was simulated. Several processing protocols that all included corrections for scatter, attenuation, and partial volume effect were compared using the simulated data. The protocol yielding the most accurate estimates of activity concentrations in the spheres was identified. This protocol was then applied to the experimental SPECT acquisitions of the cylindrical phantom and of an anthropomorphic phantom. Using the experimental data, the impact of the delineation and location of the volumes of interest (VOI) used for the measurements was also studied.

The algorithm yielding the most accurate activity estimates included a dual energy window scatter subtraction, nonuniform attenuation correction in OSEM, and partial volume effect correction using recovery coefficients. With this protocol, errors in activity estimates were less than 9% in spheres greater than 15 mm in diameter for the simulated and the experimental data of the cylindrical phantom. Realistic errors in volume delineation increased the errors in activity estimates up to 23% for these spheres. Using the anthropomorphic phantom, errors in activity estimates using realistic VOI were less than 20% in all organs and tumors.

Appropriate processing of ^{111}In SPECT images yielded clinically useful activity estimates that were accurate within $\pm 20\%$. It is therefore possible to use these activity values as an input for radiation-absorbed dose calculations in targeted radiotherapy.

Index Terms—Indium 111, quantification, single photon computed emission tomography.

I. INTRODUCTION

RECENT studies suggest that with SPECT imaging it is possible to accurately estimate radionuclide activity, distribution, and local activity concentrations if the acquisition and

processing parameters are carefully designed. In particular, it is well accepted that attenuation, scatter, partial volume effect and sometimes even motion should be compensated for, to estimate activity concentration from SPECT images with an accuracy of $\pm 10\%$ (e.g., [1] and [2]). However, our clinical experience shows that the required protocols are not yet widely available for routine clinical use. SPECT scans would have significantly greater clinical application if they could more readily systematically yield quantitative estimates of activity. For example, in targeted radiotherapy, the uptake of radiopharmaceuticals could be estimated using SPECT scans and absorbed dose calculations of a tracer with a similar biodistribution could be deduced. Several investigations have studied the quantitative accuracy that could be obtained using markers frequently used in targeted radiotherapy, mostly Iodine 131 (^{131}I) [3]–[5] and also, to a lesser extent, Indium 111 (^{111}In) [2], [6].

The purpose of this work was to study the quantitative accuracy that could be obtained in ^{111}In SPECT, using post-acquisition processing protocols readily widely available to clinicians. This might have great clinical significance in that it may allow ^{111}In SPECT to be used in the dosimetry of ZEVALIN® (ibritumomab tiuxetan) labeled with yttrium 90.

^{111}In is a gamma ray emitter with principal emissions at 171 keV and 245 keV, respectively, and has a half-life (67.9 h) comparable with that of pure β-emitter yttrium 90 (^{90}Y, 64.8 h half-life). ^{111}In-labeled agents are therefore generally used as chemical and biological surrogates to trace the biodistribution of ^{90}Y-labeled therapeutic agents [7]. ^{90}Y indeed permits efficient delivery of ionizing radiation to targeted cells while limiting radiation to normal tissue. ^{90}Y-ibritumomab tiuxetan was the first radioimmunoconjugate that has been approved by the U.S. Food and Drug Administration and the European authorities for the treatment of patients with relapsed or refractory low-grade, follicular, or transformed B-cell non-Hodgkin lymphoma (NHL), including patients with rituximab-refractory follicular lymphoma.

Few studies have evaluated the quantitative accuracy achieved with ^{111}In SPECT. Using phantom studies, Hawkins *et al.* investigated the accuracy with which organ volumes and ^{111}In activity in different regions could be estimated [8]. Their reconstruction protocol involved filtering the SPECT projections using a 2-dimensional (2D) Wiener filter to compensate for scatter and collimator blur and using the circular harmonic transform reconstruction algorithm to correct for uniform attenuation. By considering an optimal intensity threshold to
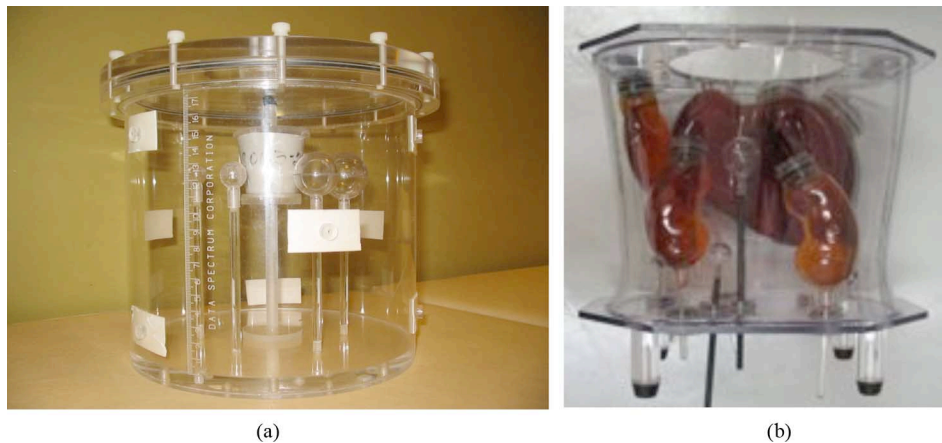
Fig. 1. Phantoms used in the study: A. Deluxe Jaszczack Phantom™ including 5 spheres and a bony insert. B. Liqui-Phil™ phantom duplicating the torso of a male from the diaphragm to the upper pelvis, and including liver, spleen, kidneys compartments, and 2 spheres mimicking tumors.

define the volumes of interest (VOI) that best matched the actual organ volumes, they could estimate regional activities in large regions (from 125 mL to 500 mL) with errors less than 12% in magnitude. The same group assessed this reconstruction protocol considering 8 normal beagle dogs [9] and reported errors less than 7.5% in both liver volume and liver activity estimates. However, these results cannot be easily extrapolated to patient studies in which scatter and attenuation are more severe than in the 10 kg dogs considered in the study. Gilland also compared the accuracy of various quantitative ^{111}In SPECT protocols, involving scatter correction, filtered-backprojection, uniform or nonuniform attenuation corrections with the non iterative Chang approach [10]. A thorax phantom was used for this investigation. Activity estimates were accurate within 16% independent of the considered protocol. More recently, Ljungberg *et al.* used Monte Carlo simulations of the anthropomorphic Zubal phantom to determine how well ^{111}In SPECT could estimate ^{111}In activity concentration in various organs, in the context of absorbed dose calculation for ^{90}Y therapy [11]. The reconstruction procedure included compensations for scatter, attenuation and distance-dependent collimator response within OSEM iterative reconstruction. Large biases in organ activity estimates were reported (from about -20% to $+50\%$), mostly because measurements were performed in anatomical volumes derived from the high-resolution CT phantom images. These measurements were therefore affected by severe partial volume effect, which was not compensated for. In addition, the simulated data ignored septal penetration, and this phenomenon cannot be neglected for ^{111}In [12]. He *et al.* [2] recently used Monte Carlo simulations and phantom experiments to assess the quantitative accuracy in activity estimates using a reconstruction protocol including corrections for scatter, attenuation, collimator response, and partial volume effect. Excellent agreement between known and estimated activity was found in various organs, with errors less than 5% in most large organs and slightly worse than 10% in a small sphere (22 mm inner diameter) and in the lung compartments. This group [6] also compared this reconstruction protocol with a simplified protocol in which only 2 conjugate projections were used to estimate the activity in 3D volumes of interest defined on CT images and co-registered with the planar images. They found that this simplified protocol was only slightly worse than the quantitative SPECT protocol in terms of accuracy.

Our study is complementary to the investigations of He *et al.* [2]. However, instead of looking at the relative impact of correcting for different phenomena (scatter, attenuation, detector response function), we only considered processing protocols including corrections for scatter, attenuation and partial volume effect (PVE) resulting from the limited detector response function. Our focus was on the accuracy of different protocols as a function of the chosen photopeak(s), the impact of VOI drawing upon quantitative accuracy, and methods for scatter and partial volume effect correction. Of particular emphasis were correction methods that could be easily implemented in the clinic with any gamma camera. The accuracy of various protocols was first evaluated using Monte Carlo simulations. As a measure of internal consistency and quantitative accuracy, the selected protocol was then applied to experimental data analogous to the Monte Carlo simulations. Finally, we applied the selected protocol to a SPECT acquisition of an anthropomorphic phantom that closely approximated a realistic clinical situation.

II. MATERIALS AND METHODS

A. Phantoms

A cylindrical phantom (Deluxe Jaszczack Phantom™, Data Spectrum Corp. NC, USA), 18.6 cm high and 22.25 cm in diameter, containing 5 spheres (inner diameters of 33.5, 28, 16, 13.5, 10.5 mm, respectively) with ^{111}In activity set to 129.5 kBq/mL was considered. A cold bone insert made of Teflon with a truncated cone shape (45 mm long, 53.5 and 37 mm in diameter at the two ends, density of $1.93\,\mathrm{g/cm^3}$) was introduced in the centre of the phantom (Fig. 1). Background activity was 15.8 kBq/mL. The sphere-to-background activity concentration ratio was 8.2. The total phantom activity was 110 MBq.

An abdominal anthropomorphic phantom (Liqui-Phil™), filled with ^{111}In was also evaluated. It contained a liver

(11.5 kBq/mL), spleen (44.4 kBq/mL), left (15.9 kBq/mL) and right (12.9 kBq/mL) kidneys and two spheres mimicking tumors (4 and 2 cm in inner diameter filled with 55.5 kBq/mL and 88.8 kBq/mL of ^{111}In). Background activity was 2.29 kBq/mL, and the total phantom activity was 53 MBq. The volumes of the various inserts are reported in Table VII. All activity values were set so as to be in the range of activity values measured in patients.

B. Experiments: SPECT and CT Acquisitions

A DST-XLi gamma camera (General Electric Medical Systems, Milwaukee, WI, USA) with a 9.5 mm thick NaI(Tl) crystal ($FOV = 540 \times 400$ mm^2) equipped with two Medium Energy High Resolution collimators (55 mm thickness, 19250 hexagonal holes with flat-to-flat distance of 3 mm, and septal thickness of 0.6 mm) was used to perform the SPECT acquisitions. Using this collimator, the spatial resolution measured by the Full Width at Half Maximum (FWHM) was 9.5 mm for a source to collimator distance of 10 cm.

For the two phantoms, 2 acquisitions were performed using 128 projections (20 seconds per projection, matrix size 128×128, pixel size $= 4.52$ mm $\times 4.52$ mm) along a circular orbit (radius of rotation $= 25.2$ cm and 31.1 cm for the cylindrical and abdominal phantoms, respectively) over 360 °. The first acquisition was performed with 4 energy windows for scatter correction using the Double Energy Window (DEW) subtraction method [13]: $[105$ keV $- 150$ keV$]$, $[156$ keV $- 186$ keV$]$, $[192$ keV $- 218$ keV$]$, and $[224$ keV $- 272$ keV$]$. The second acquisition was performed with 5 energy windows for scatter correction using the Triple Energy Window (TEW) [14]: $[150$ keV $- 156$ keV$]$, $[156$ keV $- 186$ keV$]$, $[186$ keV $- 192$ keV$]$, $[218$ keV $- 224$ keV$]$, and $[224$ keV $- 272$ keV$]$. 18.6 and 7.4 million counts in total were acquired in the two 20% windows centred on 171 and 245 keV, for the cylindrical and the abdominal phantoms, respectively.

A blank SPECT acquisition was also performed to record background activity, with the same acquisition parameters as those previously described, except the number of projections and the time per projection that were, respectively, 64 and 10 s/proj.

The inserts of the two phantoms were filled with a contrast medium (Iopamiron 300, Schering) so that they could be seen and segmented on a CT scan. The concentration was of 7 per 1000 of an iodine solution of 300 mg/ml. The entire phantoms were filled with water. CT scans of the phantoms were acquired with a LightSpeed Plus system (General Electric Medical System) with acquisition parameters of 140 kVp and 240 mA (matrix size 512×512, pixel size $= 0.84$ mm $\times 0.84$ mm, slice thickness=5 mm for the cylindrical phantom and 3.75 mm for the anthropomorphic phantom).

C. Simulations of SPECT Acquisitions

SPECT projections of the cylindrical phantom acquisition were simulated using GATE [15], which has been previously validated for ^{111}In SPECT simulations using the camera considered here [12]. The same acquisition geometry was used (same radius of rotation, same number of projections, same sampling). The energy resolution of the simulated camera was assumed to

depend on energy E with the FWHM of the energy response function at energy E given by

$$FWHM(E) = FWHM(E0)\frac{\sqrt{E0}}{\sqrt{E}}. \tag{1}$$

FWHM(E0)/E0 was set to 0.1 at energy E0 $= 245$ keV. This value was determined by analyzing the energy spectrum of a point source in air [12].

The intrinsic spatial response of the camera was partly modeled by GATE, as GATE tracks photons in the crystal. The output data were therefore only convolved using a 1.6 mm FWHM 2D Gaussian function to account for the blur introduced by the photomultiplier response and associated electronic processing [12]. To model the two emission energies of ^{111}In (171 and 245 keV), two independent simulations were performed and appropriately weighted to account for the respective frequency of the 171 and 245 keV emission rays. This approach is indeed more efficient than using the decay scheme of ^{111}In in GATE. The simulation accurately reproduced the SPECT acquisition parameters: ten billion counts were simulated, and 1.7 million counts were detected in the two 20% energy windows (i.e., the statistics was ten times less than in the corresponding experimental data).

D. Data Processing and Reconstruction

All experimental data were first corrected for background noise by subtracting the averaged blank projection of the 64 blank projections properly scaled to account for the difference in acquisition durations between the blank scan and the phantom scan. The CT and the SPECT data were registered using a method maximizing the autocorrelation between the SPECT and the CT data [16], so that the CT could be used for attenuation correction and VOI drawing. Three corrections for scatter, one for attenuation, and two for PVE were considered.

1) Scatter Correction: Three energy-based scatter correction methods that could be easily implemented on our clinical console were evaluated. All subtracted scattered photons from the projections before tomographic reconstruction.

1. Double Energy Window (DEW) subtraction method [13]: projections recorded in a $[105$ keV $- 150$ keV$]$ "scatter" window were scaled down by a factor k $= 0.21$ and subtracted from the 171 keV photopeak projections acquired in the $[156$ keV $- 186$ keV$]$ window. Similarly, projections recorded in a $[192$ keV $- 218$ keV$]$ "scatter" window were scaled down by a factor k $= 0.2$ and subtracted from the 245 keV photopeak acquired in the $[224$ keV $- 272$ keV$]$ window. The two k scaling factors were determined using the Monte Carlo simulations of the cylindrical phantom, so as to minimize the mean square difference between the photopeak projections of the scattered photons only (known as Monte Carlo simulations are used) and the scaled projections acquired in the "scatter" window.

2. Triple Energy Window (TEW) [14]: the 171 keV photopeak window $[156$ keV $- 186$ keV$]$ was corrected by using the two narrow windows ($[150$ keV $- 156$ keV$]$ and $[186$ keV $- 192$ keV$]$) located on each side of the photopeak, whereas the 245 keV photopeak window $[224$ keV $- 272$ keV$]$ was corrected using the $[218$ keV $- 224$ keV$]$

and $[272 \text{ keV} - 278 \text{ keV}]$ windows on simulated data, but using only one window ($[218 \text{ keV} - 224 \text{ keV}]$) on the experimental data.

3. Multispectral analysis (MW) method [17]. In this method, which can be regarded as an extension of the DEW approach, the scatter contribution in the projections corresponding to the 171 keV photopeak energy window is supposed to be a linear combination of the projections acquired in 3 scatter windows, while the scatter contribution in the projections corresponding to the 245 keV photopeak energy window is supposed to be a linear combination of the projections acquired in 2 scatter windows. The method was applied using the $[99 \text{ keV} - 144 \text{ keV}]$, $[144 \text{ keV} - 156 \text{ keV}]$, and $[186 \text{ keV} - 206 \text{ keV}]$ scatter windows to estimate scatter in the $[156 \text{ keV} - 186 \text{ keV}]$) photopeak window and using weighted factors k of 0.17, 0.18 and 0.18, respectively. The 245 keV photopeak window $[230 \text{ keV} - 272 \text{ keV}]$ was corrected by considering the $[206 \text{ keV} - 218 \text{ keV}]$ and $[218 \text{ keV} - 230 \text{ keV}]$ scatter windows and k = 0.15 and 0.15. The 5 k values were determined using Monte Carlo simulations of the cylindrical phantom, as explained for the DEW method.

In all scatter corrected projections, negative values were set to zero before reconstruction.

To establish a reference when comparing the scatter correction methods, projections of only the unscattered photons were also reconstructed when using the simulated data.

2) Image Reconstruction: Tomographic reconstruction was performed using the ordered-subset expectation maximization (OSEM) reconstruction algorithm [18] considering a system matrix that models non uniform attenuation. The attenuation maps were derived from the CT scans of the phantoms, by manual segmentation of the bone and soft tissue compartments and assignment of appropriate attenuation coefficients to each compartment. In the compartment filled with water, the attenuation coefficient was set to 0.145 cm^{-1} and 0.125 cm^{-1} at 171 and 245 keV, respectively. In the bone compartment (cylindrical phantom only), the attenuation coefficient was set to 0.27 cm^{-1} and 0.23 cm^{-1} at 171 and 245 keV, respectively. When summing the 171 and 245 keV projections before reconstruction (see Section D.4), averaged attenuation coefficients (0.135 cm^{-1} for water and 0.25 cm^{-1} for bone) were used, corresponding to the weighted sum of attenuation coefficients at 171 and 245 keV [19].

OSEM was used with 4 subsets and 8 iterations. The number of iterations was set so as to reach stable values in the various VOI (results not shown). The detector response function was not modeled in the system matrix.

3) Partial Volume Effect (PVE) Correction: Two PVE corrections were implemented on the reconstructed images. The first consisted in multiplying activity values measured in the VOI by the recovery coefficient (RC) corresponding to this VOI, assuming that the VOI matched the real contours of the compartment of interest [20], [21]. For the simulated data, the VOIs corresponded to the exact volume of each compartment as defined on the simulated activity map. In the real data (cylindrical and abdominal phantoms), the VOIs were obtained by manual delineation of the compartment of interest on the CT images.

For a given VOI, the RC was obtained as $1/x$, where x was the total intensity in the VOI in the image volume obtained by convolving a binary image of the VOI (1 in the VOI, 0 elsewhere) by the 3D point spread function in the reconstructed image. This point spread function was 19.2 mm full width at half maximum (FWHM) in images reconstructed from the 171 keV photopeak only, 20.3 mm FWHM in images reconstructed from the 245 keV photopeak only, and 18.1 mm FWHM in images reconstructed from the two photopeaks (see below). These values were determined by comparing the activity profile through the largest sphere of the experimental cylindrical phantom with theoretical activity profiles calculated for different spatial resolutions, given the actual size and activity of the sphere.

The second PVE correction consisted in inverting a cross-contamination (CC) matrix [1], [22]. For both phantoms, the matrix was a (7×7) matrix as there were 7 compartments in each phantom. The cross-contamination matrix entries were calculated by convolving the binary image of each compartment by a 3D stationary point spread function (see above), and by determining the percentage of signal coming from that compartment detected in the compartment and in the other compartments.

4) Selection of the Photopeaks to be Used: The processing protocol that was found to yield the most accurate activity estimates was assessed in 4 configurations: 1) "171" configuration: processing of the data recorded in the 171 keV photopeak window only; 2) "245" configuration: processing of the data recorded in the 245 keV photopeak window only; 3) "sum after (SA)" configuration: independent processing and reconstruction of the data corresponding to the two photopeak windows, then sum of the reconstructed images; and 4) "sum before (SB)" configuration: sum of the projections corresponding to the two photopeak windows and reconstruction of the resulting projections. In the SB case, scatter correction was applied to the projections before summing, and attenuation correction was performed using averaged attenuation coefficients (see Section B.2).

E. Assessment of Quantitative Accuracy

For all datasets (the simulated data and the two experimental datasets corresponding to the cylindrical and the Liqui-Phil™ phantoms, respectively), quantitative accuracy was evaluated by determining the errors in activity estimates in different compartments. Converting pixel values to activity values first required a determination of the system sensitivity. For the simulation, the system sensitivity was measured by simulating a "point" source (sphere of 1 mm in diameter) with an activity of 1 MBq. All simulation parameters were kept identical to those used for simulating the cylindrical phantom. The sensitivity of the real camera was determined by considering a cylindrical vial (2.7 cm in inner diameter and 11.5 cm in length, 57 mL volume) filled with 2.6 MBq of ^{111}In. The sensitivity was calculated by calculating the number of counts in the reconstructed images (corrected for attenuation) in a loose VOI including all the counts coming from the object (point source or vial), and by taking the ratio between this number and the actual activity.

For each compartment of the experimental cylindrical phantom (except the background), activity values were measured for 3 types of VOI, defined using a pixel size of 4.52 mm: 1) Ideal VOI (iVOI) were spherical with the exact volume of the

compartment and their location was tuned so as to maximize the number of counts detected in the VOI; 2) CT registered VOI (rVOI) were manually drawn from the CT of the experimental data after it has been registered to the SPECT data and placed back to the SPECT data; and 3) Optimized VOI (oVOI) were identical to rVOI but differed in location, as their location with respect to the compartment was optimized as for iVOI. rVOI and oVOI were not constrained to be spherical. In a clinical setting, only rVOI and oVOI are realistic. Comparing the results obtained with these VOI with the iVOI results made it possible to determine the error due to the VOI drawing only.

For all phantoms, background activity was measured by considering a small VOI far away from any other compartment.

F. Methodology for Comparing Protocols

The protocol yielding the best quantitative accuracy was first identified using the Monte Carlo simulated data. Protocols were compared by systematically considering the SB configuration. To study the impact of the scatter correction method, the 3 protocols involving the 3 scatter corrections previously described were compared, all involving the RC PVE correction. Then, to study the impact of the PVE correction method, 2 protocols involving the scatter correction that was found to be best in the previously mentioned study and the 2 PVE correction methods were compared. The scatter and PVE correction methods yielding the most accurate results were then used in the subsequent protocol comparisons. The impact of the photopeaks used for the reconstruction (171, 245, SA, or SB configurations) was studied given the scatter and PVE corrections selected as described above. All the previously described comparisons were performed for ideal VOIs defined from the simulated activity map, without errors being introduced by VOI definition and placement.

The protocol that was found to yield the most accurate results on the simulated data was then applied to the experimental data of the cylindrical phantom. Results were compared with those obtained with the simulated data, to check consistency. In addition, the impact of the VOI considered for measurement was studied, by comparing results obtained with iVOI, oVOI, and rVOI.

Finally, the selected protocol was applied to the measured data of the abdominal phantom to determine the accuracy with which activity concentration could be estimated in different anatomical regions.

Results are presented in terms of percent error in activity estimates, calculated as $100\times$ (measured activity—true activity)/ true activity. Depending on the study, results are either presented for each compartment independently, or averaged (± 1 standard deviation) over all compartments.

III. RESULTS

A. Selection of a Quantitative Protocol Using Simulated Data

1) Comparison of Scatter Correction Methods: Table I presents the errors in activity estimates as a function of the sphere inner diameter for the protocols involving the 3 different scatter corrections, all protocols including the RC PVE correction. The results were obtained for the SB configuration (see Section II-D4) and for VOI with the exact volumes and positions.

TABLE I
PERCENT ERRORS IN ACTIVITY ESTIMATES IN THE DIFFERENT COMPARTMENTS OF THE SIMULATED CYLINDRICAL PHANTOM, AS A FUNCTION OF THE SCATTER CORRECTION METHOD. ALL DATA WERE CORRECTED FOR PVE USING RC, THE TWO PHOTOPEAKS WERE USED AND THE VOI USED FOR MEASUREMENTS HAD THE EXACT SIZE AND LOCATION

Sphere diameter (mm)	DEW	TEW	MW	unscattered
33.5	7	-12	3	10
28	9	-15	4	15
16	0	-12	-7	-2
13.5	0	-17	-6	4
10.5	-35	-54	-41	-24
Background	13	-12	6	4
Mean ± 1 sd	-1 ±18	-20 ±17	-7 ±18	1 ±14

TABLE II
PERCENT ERRORS IN ACTIVITY ESTIMATES IN THE DIFFERENT SPHERES OF THE SIMULATED CYLINDRICAL PHANTOM, AS A FUNCTION OF THE PVE CORRECTION METHOD. ALL DATA WERE CORRECTED FOR SCATTER USING DEW, THE TWO PHOTOPEAKS WERE USED AND THE VOI USED FOR MEASUREMENTS HAD THE EXACT SIZE AND LOCATION.

Sphere diameter (mm)	RC	CC
33.5	7	8
28	9	9
16	0	-2
13.5	0	-2
10.5	-35	-35
Mean ± 1 sd	-4±18	-4±18

When combined with RC PVE correction and when using the 2 photopeaks, both DEW and MW scatter corrections yielded results that were not significantly different from those obtained using the unscattered photons only ($p > 0.01$, paired t-test corrected for multiple comparisons), unlike TEW. Although contrasts between spheres and background were well restored using TEW (results not shown), TEW introduced a systematic underestimation of activity, as previously described in ^{201}Tl configurations [23]. This is because the positioning of the TEW narrow windows was not optimized for our setting, and these windows included a significant proportion of unscattered photons (more than 20% of the detected photons in the $[186 - 192 \text{ keV}]$ for instance). Because DEW is easier to implement in clinical routine than MW or optimized TEW, it was then used for all subsequent protocols performed with simulated data.

2) Comparison of PVE Correction Methods: Table II presents the errors in sphere activity estimates for the protocols involving 2 different PVE corrections, all protocols including the DEW scatter correction. The results were obtained for the SB configuration and for the VOIs with the exact volumes and positions.

Table II suggests that the two PVE correction methods performed similarly in this simple phantom configuration (paired t-test, NS). This was not surprising as the CC method is expected

TABLE III
PERCENT ERRORS IN ACTIVITY ESTIMATES IN THE DIFFERENT COMPARTMENTS OF THE SIMULATED CYLINDRICAL PHANTOM, AS A FUNCTION OF THE PHOTOPEAK DATA THAT WERE CONSIDERED. ALL DATA WERE CORRECTED FOR SCATTER USING DEW AND FOR PVE USING RC. THE VOI USED FOR MEASUREMENTS HAD THE EXACT SIZE AND LOCATION

Sphere diameter (mm)	171	245	SA	SB
33.5	14	-2	10	7
28	14	6	11	9
16	14	-5	0	0
13.5	8	11	0	0
10.5	-26	-10	-28	-35
Background	15	-7	16	13
Mean ± 1 sd	6 ±16	-1 ±8	2 ±16	-1 ±18

TABLE IV
PERCENT ERRORS IN ACTIVITY ESTIMATES IN THE DIFFERENT SPHERES OF THE EXPERIMENTAL CYLINDRICAL PHANTOM FOR THE PROCESSING PROTOCOL INVOLVING THE DEW SCATTER CORRECTION, ATTENUATION CORRECTION AND THE RC PVE CORRECTION. THE 2 PHOTOPEAKS WERE USED AND THE VOI USED FOR MEASUREMENTS HAD THE EXACT SIZE AND LOCATION

Sphere diameter (mm)	% errors
33.5	-4
28	8
16	19
13.5	-7
10.5	48
Background	7
Mean ± 1 sd	12±20

TABLE V
PERCENT ERRORS IN ACTIVITY ESTIMATES IN THE DIFFERENT COMPARTMENTS OF THE EXPERIMENTAL CYLINDRICAL PHANTOM FOR THE SELECTED QUANTITATIVE PROTOCOL, AS A FUNCTION OF THE VOI USED FOR THE MEASUREMENTS

Sphere diameter (mm)	iVOI	oVOI	rVOI
33.5	-4	9	10
28	8	21	21
16	19	-4	-7
13.5	-7	-18	-35
10.5	48	-28	-57
Mean ± 1 sd	13±22	-4±20	-14±32

to be more accurate than the RC method in configurations where hot structures are surrounded by a variety of structures with different uptakes, which was not the case in our phantom. The RC method was subsequently used as it is easier to implement in clinical routine. The fact that the error depended on the sphere size (larger errors for bigger spheres) suggests that the PVE correction was not ideal. One reason might be an incorrect estimate of the spatial resolution in the reconstructed images. This spatial resolution was indeed estimated approximately from the largest sphere and was considered to be stationary, while it is not when using iterative reconstruction. The largest underestimation observed for the smallest sphere might be due partly to noise, given that the corresponding VOI included only 6 voxels.

3) Impact of the Considered Photopeak: Table III presents the errors in sphere activity estimates for the protocols involving the DEW scatter correction and the RC PVE correction, as a function of the photopeaks that were used (see Section II-D4). Results were obtained for the VOIs with the exact volumes and positions.

Table III shows that using the two photopeaks did not significantly deteriorate the quantitative accuracy with respect to using one photopeak only (the only significant difference with $p < 0.05$ was the percent errors with SB significantly smaller than those when using the 171 keV photopeak only, paired t-test corrected for multiple comparisons). The way data corresponding to the two photopeaks were combined did not change quantitative accuracy either (paired t-test, $p > 0.05$). Because summing projections before reconstruction simplifies processing, the SB configuration was systematically used thereafter.

Given the results obtained using the simulated data, the protocol involving the DEW scatter correction, the RC PVE correction, and the sum of the scatter-corrected projections before reconstruction (SB) was considered for further assessment on experimental data.

B. Application of the Selected Protocol to Measured Phantom Data

1) Cylindrical Phantom: Table IV shows the percent errors in activity estimates for the selected protocol involving the DEW scatter correction, attenuation correction and the RC PVE correction for the experimental SPECT/CT of the cylindrical

phantom. The results were obtained using the SB configuration and for the iVOI.

Results from Table IV are not identical to but are of the same order of magnitude as those found with the simulated data corresponding to the same experimental set up (last column in Table III). The mean difference between percent errors observed for the simulated (last column of Table III) and the experimental data (Table IV) was not significantly different (paired t-test). The large magnitude of the error associated with the smallest sphere might be due to the large CT slice thickness, introducing sampling errors when using the CT for attenuation and PVE corrections. In addition, the activity estimates in the smallest sphere were noisy, as the VOI included only 6 voxels.

Table V shows the percent errors in activity estimates for the selected protocol applied to the experimental SPECT/CT of the cylindrical phantom for the three types of VOI.

Table VI gives the percent differences in VOI volumes with respect to the actual volumes of the spheres for the iVOI and oVOI (oVOI and rVOI had the same volumes).

Table V clearly demonstrates that the definition and location of the VOI had a high impact on quantitative accuracy. Table VI suggests that for the largest spheres (33 and 28 mm in diameter), the sphere volumes tended to be overestimated, which yielded

TABLE VI
PERCENT DIFFERENCES BETWEEN VOI VOLUMES AND ACTUAL SPHERE VOLUMES FOR THE iVOI, rVOI AND oVOI VOLUMES OF INTEREST

Sphere diameter (mm)	iVOI	oVOI/rVOI
33.5	-4.7	28.6
28	-1.1	37.4
16	3.3	-9.6
13.5	0.4	-14
10.5	6.6	-39
Mean ± 1 sd	1±4	1±32

TABLE VII
PERCENT ERRORS IN ACTIVITY ESTIMATES IN THE DIFFERENT COMPARTMENTS OF THE EXPERIMENTAL ABDOMINAL PHANTOM FOR THE SELECTED QUANTIFICATION PROTOCOL. ALL DATA WERE CORRECTED FOR SCATTER, ATTENUATION AND PVE. THE TWO PHOTOPEAKS WERE USED AND THE oVOI WERE CONSIDERED FOR MEASUREMENTS. PERCENT ERRORS IN COMPARTMENT VOLUME ESTIMATES ARE ALSO SHOWN WITH TRUE VOLUMES SHOWN IN PARENTHESIS

Compartment	% error in activity estimates	% error in volume estimates (true volume in mL)
Liver	8	0.2 (1594)
Spleen	10	2.3 (170)
Left kidney	3	0.1 (116)
Right kidney	17	0.5 (144)
40 mm sphere	1	0.1 (33.5)
20 mm sphere	20	1.7 (4.2)
Background	16	N/A (9000)
Mean ± 1 sd	11 ± 7	0.8 ± 0.9

overall activity overestimation in these spheres (Table V). For small spheres, the smaller the sphere, the more underestimated the volume, and the greater the activity underestimation. This may reflect a different strategy in drawing VOI as a function of the apparent object size. Note also that the ideal VOI did not always yield the most accurate activity estimates. This might be due to incidental compensation of errors introduced at different levels (in VOI drawing, in attenuation or scatter or PVE corrections), and also to noise and sampling effects (especially for the smallest sphere).

2) Abdominal Phantom: Table VII shows the percent errors in activity estimates for the selected protocol applied to the experimental SPECT/CT of the abdominal phantom, with the oVOI used for measurements. The table also shows the error in volume estimates observed when considering the oVOI. These latter errors were actually slightly smaller than those observed for the cylindrical phantom (Table VI). This is probably because the organs were larger than the spheres of the cylindrical phantom, and also because the CT slice thickness was smaller for the anthropomorphic phantom than for the cylindrical phantom. Thinner CT slices improved the accuracy of the contour delineation. Note also that the errors in activity estimates were different in the two kidneys, although they had similar sizes and activities. This might be because their locations with respect to other organs were different. Overall, the activity estimates tended to be overestimated. This suggests that the spatial resolution parameters (see Section II-D3) used for partial volume effect correction did not match perfectly the actual spatial resolution in the reconstructed images of the abdominal phantom. Indeed, these parameters were optimized for the cylindrical phantom, but the speed of convergence of the iterative reconstruction algorithm, hence the spatial resolution in the reconstructed image, are also dependent on the object being reconstructed (activity distribution and propagation media). The spatial resolution parameters were thus only approximate for the abdominal phantom. Another possible explanation for this activity overestimation could be an underestimation of the k values used in DEW, as these were optimized for the cylindrical phantom which corresponds to a smaller scattering volume than the abdominal phantom.

IV. DISCUSSION

Overall, our results suggest that reasonable accuracy in activity estimates can be obtained in ^{111}In SPECT, providing that the data are corrected for scatter, attenuation and PVE. These results confirm those by He *et al.* [2], [6] but they additionally show that even with correction methods that are simple to implement (DEW for scatter correction, recovery coefficients for PVE correction, modeling attenuation in OSEM), activity can be estimated with errors less than 20%, except in the smallest structures (spheres less than 20 mm in diameter in our study). These conclusions suggest that accurate quantification of ^{111}In SPECT can be achieved in clinical centers.

Our study identified an acquisition and processing protocol that results in good quantitative accuracy for ^{111}In SPECT. First, to filter background activity from our experimental data we systematically acquired a blank scan that was subtracted from the experimental scan after rescaling for difference in acquisition duration. However, we found that this background subtraction could be optional, as less than 1% of the total registered counts was due to background activity.

Second, our protocol involved the DEW scatter correction, which appeared to be accurate enough in our configuration. The performance of two more sophisticated scatter correction methods (TEW and MW) have also been characterized. The TEW correction yielded a systematic underestimation of activity, consistent with what was previously reported for non ^{99m}Tc data [23] and partially explained by the non optimal positioning of the narrow windows that still included a significant amount of unscattered photons (up to 20% in the [186 − 192 keV] energy window). On experimental data, TEW was based on one scatter window only for the 245 keV photopeak due to a limitation in the number of spectral windows that could be simultaneously defined on our acquisition console [24]. However, using simulated data, we found that the number of counts detected in the high energy scatter window (that was omitted in our experimental data) was less than 0.8% of that detected of the low energy scatter window associated with the

245 keV photopeak. Our experimental implementation of TEW was therefore not expected to introduce substantial additional bias compared to the classical implementation. To reduce the noise amplification introduced by considering narrow energy windows to estimate scatter, we also used 6 keV wide secondary windows as suggested by Ogawa *et al.* [14]. One way to improve the performance of TEW for ^{111}In imaging might be to optimize the width and location of the narrow windows, although this is not very practical (8 parameters to be optimized). The MW method appeared quite accurate, but is more difficult to implement on clinical machines than DEW, without a significant increase in accuracy. Overall, despite its well known weaknesses (for instance, dependence of k on the object size, need to calibrate k as a function of the detector energy resolution and energy windows), DEW was found to have the best trade-off between ease of implementation and accuracy.

Regarding attenuation correction, we modeled attenuation in the system matrix used for tomographic reconstruction, based on a prior attenuation map. The main obstacle for the practical feasibility of this approach is the availability of an accurate enough attenuation map. This is possible using conventional transmission devices [25] or SPECT/CT systems [26].

In this work, we did not directly correct for the distance dependent collimator response, but only addressed the consequences of the limited spatial resolution in the reconstructed images using PVE correction. Given that compensation for distance dependent collimator response are now becoming commercially available, they should be recommended as a mean to 1) reduce PVE by improving the reconstructed spatial resolution and 2) make the spatial resolution more stationary in the reconstructed images. However, although this compensation reduces PVE, this effect remains significant in the reconstructed images and still needs to be corrected.

PVE is certainly one of the most difficult sources of bias to deal with in modern clinical practice. Various PVE corrections have been described, with very encouraging results (e.g., [1], [20], [21], [27], and [29]). Among these methods, the simplest is the scaling of values measured in specific regions using a recovery coefficient [20], [27]. This can be easily calculated if the volume of the structure of interest and the spatial resolution in the reconstructed images are known. When comparing this simple method with the more sophisticated method of cross-contamination matrix [22], we found that RC gave satisfactory results. When using the CC correction method instead of the RC correction method for the Liqui-Phil phantom, which was more realistic than the cylindrical phantom, we did not find any significant difference in terms of percent errors in activity estimates either (paired t-test, results not shown). This might be because the considered volumes of interest had homogeneous uptake, the surrounding activity was homogeneously distributed, and the different compartments of the phantoms were not too close. The cross-contamination method might be more accurate than the RC method for lesions at the interface of at least two organs with different uptakes, which was not the case for our two phantoms.

Although the RC method had the potential to properly correct for partial volume effect, the results were sensitive to the proper delineation and location of the VOI. One way to circum-vent the problem of VOI placement can be to roughly locate the VOI around the volume of interest, and then automatically find the position that maximizes (or minimizes for cold regions) the number of counts in that VOI, and hence includes most of the signal coming from the VOI (what we called oVOI in our study). This makes the results dependent only on the delineation of the VOI, but no longer on its accurate positioning. The approach most commonly used to delineate VOI is to use CT (or MR) images because of their much higher spatial resolution than SPECT images. Procedures that do not rely on the identity between the anatomical and functional contours are still needed. Drawing loose VOI around the organ of interest to include all activity coming from the organ is not realistic in most applications where most organs of interest are close to another organ with a different nonzero activity.

Finally, when considering ^{111}In SPECT imaging, a relevant question to consider is which photopeak should be used. Our results are consistent with previous results [10], [11] suggesting that similar accuracy is achieved using either 1 or 2 photopeaks. We therefore recommend the use of 2 photopeaks to reduce noise, hence facilitate VOI positioning on the reconstructed images. The difference in resolution that we observed between the data acquired in the two different photopeak windows is probably due to the difference in statistics in these windows: the highest spatial resolution was obtained when combining the two photopeak windows (data with the highest statistics), and the poorest spatial resolution was obtained for the 245 keV photopeak window, which is the window with the lowest statistics. A proper estimate of the spatial resolution is therefore important for the accuracy of PVE correction.

Although our results suggest that reasonable quantitative accuracy (errors less than 20%) in organ or tumor activity estimates can be obtained using clinically feasible ^{111}In SPECT protocols, there are limitations that should be mentioned. First, motion was not considered, and it is likely that accuracy in activity estimates would be poorer for moving organs or tumors. Second, we considered piecewise activity distributions, and the proposed protocol does not address quantification at a voxel level, but only at an organ or tumor level, assuming uptake is uniform within the organ or tumor. Although this might be a crude approximation in some instances, it can still be useful to compute the mean radiation-absorbed dose to organs at risk and to the tumor. Finally, the reproducibility of quantitative accuracy over a broad range of gamma cameras and test objects, and possibly patients should still be fully characterized. As a first step, it is important to stress that before any imaging and quantification protocol is used in the clinics, its accuracy should be carefully characterized using phantom acquisitions, and systematically reported prior to clinical implementation of studies relying on quantitative measurements.

V. CONCLUSION

Using simulations and phantom acquisitions, we have identified a clinically feasible data processing protocol, yielding maximum errors in activity estimates for organs or tumors of approximately 20%. This protocol involves a dual window scatter correction, nonuniform attenuation correction, partial volume correction using recovery coefficients and it takes advantage of the

two photopeaks of ^{111}In. We have also shown that VOI drawing and positioning are two key steps for achieving accurate quantification. Our results provide insight into the potential and limitations of ^{111}In SPECT quantitative imaging for radiation-absorbed dose calculation in targeted radiotherapy, and may provide clinicians with a useful tool for the quantitative assessment of radiopharmaceutical uptake.

ACKNOWLEDGMENT

REFERENCES

[1] M. Soret, P. M. Koulibaly, J. Darcourt, S. Hapdey, and I. Buvat, "Quantitative accuracy of dopaminergic neurotransmission imaging with 123I SPECT," *J. Nucl. Med.*, vol. 44, pp. 1184–1193, 2003.

[2] B. He, Y. Du, X. Song, W. P. Segars, and E. C. Frey, "A Monte Carlo and physical phantom evaluation of quantitative In-111 SPECT," *Phys. Med. Biol.*, vol. 50, pp. 4169–4185, 2005.

[3] Y. K. Dewaraja, M. Ljungberg, and K. F. Koral, "Accuracy of I-131 tumor quantification in radioimmunotherapy using SPECT imaging with an ultra-high-energy collimator: A Monte Carlo study," *J. Nucl. Med.*, vol. 41, pp. 1760–1767, 2000.

[4] Y. K. Dewaraja, S. J. Wilderman, M. Ljungberg, K. F. Koral, K. Zasadny, and M. S. Kaminiski, "Accurate dosimetry in 131I radionuclide therapy using patient-specific, 3-dimensional methods for SPECT reconstruction and absorbed dose calculation," *J. Nucl. Med.*, vol. 46, pp. 840–849, 2005.

[5] M. Ljungberg, K. Sjogreen, X. Liu, E. Frey, Y. K. Dewaraja, and S. E. Strand, "A three dimensional absorbed dose calculation method based on quantitative SPECT for radionuclide therapy. Evaluation for I-131 using Monte Carlo simulation," *J. Nucl. Med.*, vol. 43, pp. 1101–1109, 2002.

[6] B. He and E. C. Frey, "Comparison of conventional, model-based quantitative planar, and quantitative SPECT image processing methods for organ activity estimation using In-111 agents," *Phys. Med. Biol.*, vol. 51, pp. 3967–81, 2006.

[7] S. Vallabhajosula *et al.*, "Prediction of myelotoxicity based on bone marrow radiation-absorbed dose: Radioimmunotherapy studies using ^{90}Y- and ^{177}Lu-labeled J591 antibodies specific for prostate-specific membrane antigen," *J. Nucl. Med.*, vol. 46, pp. 850–858, 2005.

[8] W. G. Hawkins, N. C. Yang, and P. K. Leichner, "Validation of the circular harmonic transform (CHT) algorithm for quantitative SPECT," *J. Nucl. Med.*, vol. 32, pp. 141–150, 1991.

[9] P. Leichner, H. M. Vriesendorp, W. G. Hawkins, S. M. Quadri, N. C. Yang, R. L. Stinson, D. P. Loudenslager, T. L. Frankel, X. Chen, and J. L. Klein, "Quantitative SPECT for Indium-11-labeled antibodies in the livers of beagle dogs," *J. Nucl. Med.*, vol. 32, pp. 1442–1444, 1991.

[10] D. R. Gilland, R. J. Jaszczak, T. G. Turkington, K. L. Greer, and R. E. Coleman, "Quantitative SPECT imaging with Indium-111," *IEEE Trans. Nucl. Sci.*, vol. 38, pp. 761–766, 1991.

[11] M. Ljungberg, E. Frey, K. Sjögreen, X. Liu, Y. Dewaraja, and S. E. Strand, "3D absorbed dose calculations based on SPECT: Evaluation for 111-In/90-Y therapy using Monte Carlo simulations," *Cancer Biother. Radiopharm.*, vol. 18, pp. 99–107, 2003.

[12] K. Assié, I. Gardin, P. Vera, and I. Buvat, "Validation of the Monte Carlo simulator GATE for Indium-111 imaging," *Phys. Med. Biol.*, vol. 50, pp. 3113–3125, 2005.

[13] R. J. Jaszczak, C. E. Floyd, and R. E. Coleman, "Scatter compensation techniques for SPECT," *IEEE Trans. Nucl. Sci.*, vol. 32, pp. 786–793, 1985.

[14] K. Ogawa, Y. Harata, T. Ichihara, A. Kubo, and T. Hashimoto, "A practical method for position-dependent compton-scattered correction in single photon emission CT," *IEEE Trans. Nucl. Sci.*, vol. 10, pp. 408–412, 1991.

[15] S. Jan *et al.*, "GATE: A simulation toolkit for PET and SPECT," *Phys. Med. Biol.*, vol. 49, pp. 4543–4561, 2004.

[16] L. Junck, J. G. Moen, G. D. Hutchins, M. B. Brown, and D. E. Kuhl, "Correlation methods for the centering, rotation and alignment of functional brain images," *J. Nucl. Med.*, vol. 31, pp. 1220–1226, 1990.

[17] H. Vija, M. S. Kaplan, and D. R. Haynor, "Simultaneous estimation of SPECT activity and attenuation distributions from measured phantom data using a differential attenuation method," in *Proc. IEEE Nucl. Sci. Symp. Conf. Rec.*, 1999, vol. 2, pp. 884–888.

[18] H. M. Hudson and R. S. Larkin, "Accelerated image reconstruction using ordered subsets of projection data," *IEEE Trans. Med. Imaging*, vol. 13, pp. 601–609, 1994.

[19] Y. Seo, K. H. Wong, and B. H. Hasegawa, "Calculation and validation of the use of effective attenuation coefficient for attenuation correction in In-111 SPECT," *Med. Phys.*, vol. 32, pp. 3628–3635, 2005.

[20] R. M. Kessler, J. R. Ellis, and M. Eden, "Analysis of emission tomographic scan data: Limitations imposed by resolution and background," *J. Comput. Assist. Tomogr.*, vol. 8, pp. 514–522, 1984.

[21] N. Avril, S. Bense, S. I. Ziegler, J. Dose, W. Weber, C. Laubenbacher, W. Romer, F. Janicke, and M. Schwaiger, "Breast imaging with fluorine-18-FDG PET: Quantitative image analysis," *J. Nucl. Med.*, vol. 38, pp. 1186–1191, 1997.

[22] O. G. Rousset, Y. Ma, and A. C. Evans, "Correction for partial volume effects in PET: Principle and validation," *J. Nucl. Med.*, vol. 39, pp. 904–911, 1998.

[23] Y. Narita, H. Iida, S. Ebert, and T. Nakamura, "Monte Carlo evaluation of accuracy and noise properties of two scatter correction methods for 201TL cardiac SPECT," *IEEE Trans. Nucl. Sci.*, vol. 44, pp. 2465–2472, 1997.

[24] T. Ichihara, K. Ogawa, N. Motomura, A. Kubo, and S. Hashimoto, "Compton scatter compensation using the triple-energy window method for single- and dual-Isotope SPECT," *J. Nucl. Med.*, vol. 34, pp. 2216–2221, 1993.

[25] H. Zaidi and B. Hasegawa, "Determination of the attenuation map in emission tomography," *J. Nucl. Med. 44*, pp. 291–315, 2003.

[26] Y. Seo, K. H. Wong, M. Sun, B. L. Franc, R. A. Hawkins, and B. H. Hasegawa, "Correction of photon attenuation and collimator response for a body-contouring SPECT/CT imaging system," *J. Nucl. Med.*, vol. 46, pp. 868–877, 2005.

[27] Y. Du, B. M. W. Tsui, and E. Frey, "Partial volume effect compensation for quantitative brain SPECT imaging," *IEEE Trans. Med. Imaging*, vol. 24, pp. 969–976, 2005.

[28] L. Geworski, B. Knoop, M. de Cabrejas, W. H. Knapp, and D. L. Munz, "Recovery correction for quantitation in emission tomography: A feasibility study," *Eur. J. Nucl. Med.*, vol. 27, pp. 161–169, 2000.

[29] N. Boussion, M. Hatt, F. Lamare, Y. Bizais, A. Turzo, C. C.-L. Rest, and D. Visvikis, "A multiresolution image based approach for correction of partial volume effects in emission tomography," *Phys. Med. Biol.*, vol. 51, pp. 1857–1876, 2006.